Available online at www.sciencedirect.com
ScienceDirect
Journal of the European Ceramic Society 28 (2008) 1143–1148
www.elsevier.com/locate/jeurceramsoc

Particle in-flight behavior and its influence on the microstructure and mechanical properties of plasma-sprayed Al_2O_3 coatings

Zhijian Yin [a,b], Shunyan Tao [a,*], Xiaming Zhou [a], Chuanxian Ding [a]

[a] *The Key Laboratory of Inorganic Coating Materials, Shanghai Institute of Ceramics, Chinese Academy of Sciences, Shanghai 200050, PR China*
[b] *Graduate School of the Chinese Academy of Sciences, Beijing 100039, PR China*

Received 25 June 2007; received in revised form 5 September 2007; accepted 15 September 2007
Available online 19 November 2007

Abstract

This paper aims to elaborate the particle characteristics during their flight into the spray and its significance in determining the microstructure and mechanical properties of resultant coatings. Study of plasma spraying of Al_2O_3 using three different grain fractions of feedstock was done by an on-line monitoring system (SprayWatch 2i). The as-sprayed coatings were characterized in terms of the microstructure and composition, microhardness, adhesion strength and porosity. In addition, a statistic study of Weibull analysis was employed to further examine the microstructural homogeneity of coatings. It was found that particle in-flight behaviors are strongly influenced by feedstock particle size. Improved particle velocity and temperature as well as melting extent can be obtained for the finer feedstock. This contributes to produce increasingly bonded splats resulting in coating with compact microstructure, where low porosity and increased microhardness and adhesion strength were realized.

Keywords: Plasma spraying; Al_2O_3 coating; In-flight behavior; Microhardness; Adhesion strength

1. Introduction

Plasma spraying technique has been widely employed to produce varieties of protective coatings for wear, corrosion and heat resistance.[1–4] A plasma-sprayed coating is built up, and the microstructure is formed, when individual, fully or partially molten droplets, traveling at a particular velocity, flatten, adhere and solidify on impact to the target substrate.[5,6] The particle velocity and the temperature at impact have a strong influence on the level of flattening and adherence of the particles, which in turn influences the solidification rate and ultimately the microstructure. Thus, it is generally accepted that the velocity and temperature of in-flight particle are two of the most key parameters influencing the microstructure and properties of coatings.[7,8]

In recent years, with the development of detection technology, especially the application of CCD technology in plasma spraying, the interest in on-line diagnostic methods for thermal spraying has been increasing. The particle in-flight characteristics have proved to be sensitive to numerous factors including not only the adjustable spray parameters (e.g. the flow rate of plasma gas and electrical current)[9,10] and the nonadjustable noise factors like the wear of the electrodes.[7] Fang et al.[9] showed that the particle in-flight velocity increased remarkably with the increase of the argon flow rate, whereas the particle surface temperature was mainly influenced by the hydrogen flow rate and the increasing electrical current resulted in the increase of the particle temperature and velocity to some extent. Similar findings were obtained by Guessasma et al.[10] Furthermore, it was pointed out that the melting state of the particle, affected by the particle in-flight behavior, could be employed to analysis of the deposit structure and properties.[9] Zhao et al.[7] suggested that the wear of the electrodes led to a change in the effective plasma power and the particle in-flight properties, influencing also directly the deposition efficiency of the powder during spraying.

However, from the schematic showing of the atmospheric plasma spraying process and coating deposition in Fig. 1, it can be recognized that besides of the aforementioned adjustable spray parameters and nonadjustable noise factors, the feedstock particle characteristics (i.e. size, morphology and chemistry) also play an important role in determining the plasma particles interaction and the deposit properties and performances.

* Corresponding author. Tel.: +86 21 52414101; fax: +86 21 52413903.
E-mail address: shunyantao@mail.sic.ac.cn (S. Tao).

0955-2219/$ – see front matter © 2007 Elsevier Ltd. All rights reserved.
doi:10.1016/j.jeurceramsoc.2007.09.050

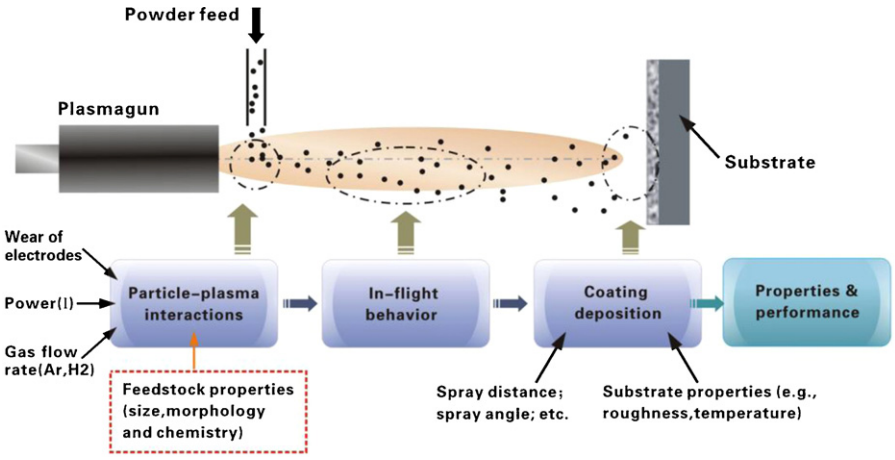

Fig. 1. The schematic diagram showing the atmospheric plasma spraying process and coating deposition.

A limited number of studies have considered the significance of feedstock powder characteristics and its effect on in-flight particle behavior and resulting coating microstructure and properties.[8,11] Within this work the characteristics of three different grain fractions of Al_2O_3 feedstock with similar morphology was examined and compared with respect to their in-flight particle characteristics during plasma spray using an on-line monitoring system (SprayWatch 2i, OSEIR, Finland). The microstructure of as-sprayed coatings was characterized by scanning electron microscopy (SEM), X-ray diffraction (XRD) and Weibull statistics analysis. The indentation and tensile tests were done to evaluate the microhardness and adhesion strength of coatings. Also, the establishment of a better understanding of particle in-flight behavior—ultimate coating microstructure (porosity, pore morphology, size and distribution)–mechanical properties relationship was attempted.

2. Experimental procedure

2.1. Materials and preparation

The Metco A-2000 atmospheric plasma spraying equipment with a F4-MB plasma gun (Sulzer Metco AG, Switzerland) was applied to deposit coatings. Three commercially available Al_2O_3 starting powders denoted as F, M and C were used as feedstock. They were all mechanically fused and crushed powders and identically contain pure α-Al_2O_3 phase. The feedstock powders were fed with a Twin-System 10-C (Plasma-Technick AG, Switzerland). The medium size (D_{50}) of these starting powders is 15.3 μm, 19.4 μm and 33.5 μm, respectively. According to the SEM analysis results, as shown in Fig. 2(a)–(c), the as-received powders display angular and irregular morphology. A mixture of argon and hydrogen was used as plasma gas. Also, the former gas was employed to act as carrier gas. Compressed air was used as substrate cooling gas during plasma spraying. In Table 1 are summarized the plasma spray parameters. Prior to spraying, the stainless steel substrates were degreased ultrasonically in acetone and grit blasted with corundum.

Table 1
Summary of the operating spray parameters

Parameters	Value	Unit
Arc current	660	A
Primary plasma gas (Ar)	49	slpm[a]
Auxiliary plasma gas (H_2)	12	slpm
Carrier gas (Ar)	3.5	slpm
Spray distance	110	mm
Nozzle diameter	6	mm
Powder inject diameter	1.8	mm

[a] Standard liters per minute.

2.2. Diagnostic of in-flight particles

During spraying, the in-flight velocity and temperature of particles prior to impact onto target substrate were measured using

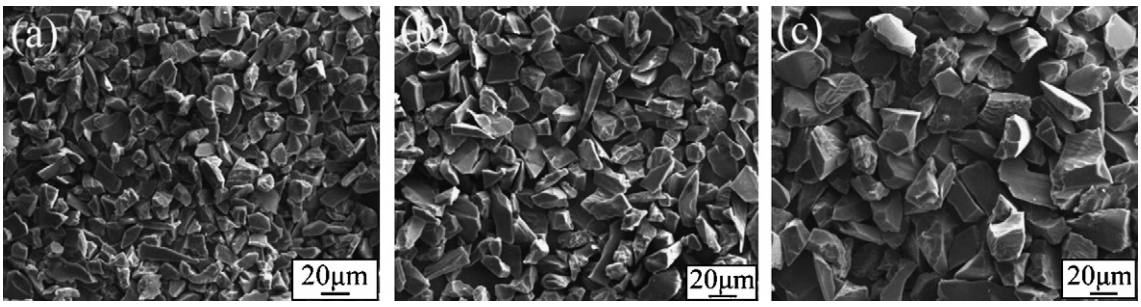

Fig. 2. SEM micrographs of as-received F (a), M (b) and C (c) feedstock powders.

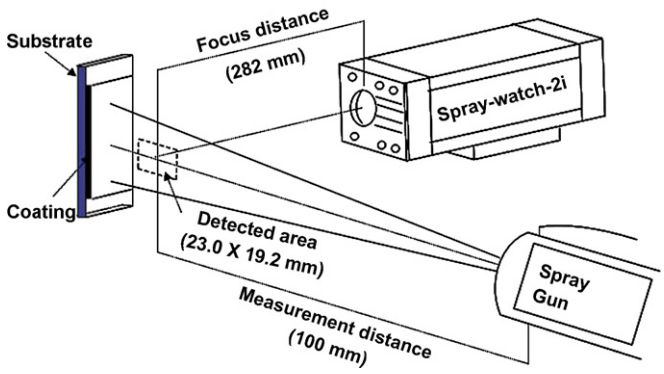

Fig. 3. The schematic view of the SprayWatch system.

on-line monitoring system (SprayWatch 2i, OSEIR, Finland). It is based on a digital CCD camera and special spectrally resolving optics (pat. pending). The optics, together with the computer control of the camera and a dedicated image processing software enables on-line measurement of the velocity and temperature of in-flight particles. The schematic view of the SprayWatch system is shown in Fig. 3. The center of the detected area is 100 mm from the nozzle exit in the axes direction. The in-flight particle velocity is calculated by a time-of-flight method. The spray is imaged using a short exposure time (typically 5–10 ms), which corresponds to 20–60 pixels on the CCD detector. During this period of time the particle traveled a certain distance. A special image-processing algorithm is used to detect the particles traces in the image, to measure their lengths and angles and to calculate the velocity of the particle in the image. The CCD collecting system was partly covered by two optical filter stripes, which allowed the measurement of the radiation intensity of the particle flow in two wavelength ranges. Thus, the in-flight particle temperature could be calculated through the two-color pyrometry method. It should be noted that for the determination of the particle temperature diagnostic systems are restricted to the analysis of surface temperature of the particles. Along the diameter of the particles exposed to the hot gas jet a temperature gradient will be present, so that knowledge of the surface temperature provides only limited information about the melting degree. To further investigate the particle melting extent, coating samples were analyzed by X-ray diffraction (XRD, RAX-10 X-ray diffractometer, Rigaku, Japan) operating with Cu Kα ($\lambda = 1.54056$ Å) radiation.[7,12]

2.3. Specimens characterization

The microstructure of as-sprayed coatings was determined using scanning electron microscopy (EPMA-8705QH2, Shimadzu, Japan). Porosity of the coatings was estimated by quantitative image analysis (IA). Ten fields are selected for the measurement of porosity. The versatility of IA method for microstructural quantification has been investigated for diverse coatings with distinct spray process and materials feedstock characteristics.[13–15] The microhardness measurements were conducted on cross-sections of coatings using a HX-1000 Microhardness Test under a load of 1.96 N with a dwell time of 15 s. Each measurement series comprised 20 readings, which were randomly located along the central region of cross-section. To avoid the effect of stress field, the distance between two indentations was kept greater than three times of the indentation diagonal. Adhesion strength of coatings was evaluated by tensile adhesion tests (Instron 5592).[16] The ASTM standard[17] was used as guidance. Five measurements were performed to determine the average value of tensile adhesion strength for each coating.

3. Results and discussion

3.1. Particle in-flight behavior

Particle in-flight behavior monitoring results are presented graphically in Fig. 4, where the in-flight velocity and temperature of Al_2O_3 feedstock powders with different particle size are plotted as a function of the monitoring time. It clearly reveals that the F particles have a high average velocity up to 405 m/s, whereas M and C particles exhibit relatively low velocity of 382 m/s and 345 m/s, respectively (Fig. 4(a)). During spraying, in-flight particles injected into plasma jet interact with the ionized plasma gas (Fig. 1). It is suggested the momentum transferred from the plasma gas to the particles shows high dependence on the mass of the injected particle.[18] Thus, the coarser (heavier) particles attain a lower velocity as compared with the finer ones. The similar trend of the in-flight temperature variation with the particle size is illustrated in Fig. 4(b) that the smaller particles exhibit higher in-flight temperature than the larger ones. This is consistent with the statistical analysis and modeling results by Friis et al.[19] and Wan et al.[20] The difference of in-flight temperature between the larger and smaller particle groups can be attributed to two factors: the different trajectories of the injected particles

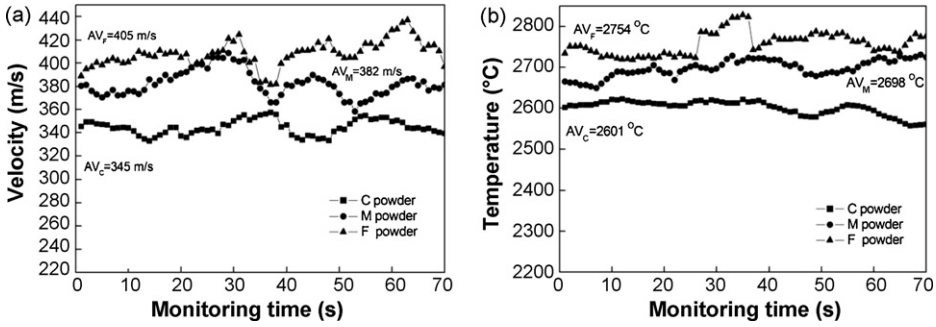

Fig. 4. In-flight particle velocity (a) and temperature (b) of feedstock with different particle size as a function of the monitoring time.

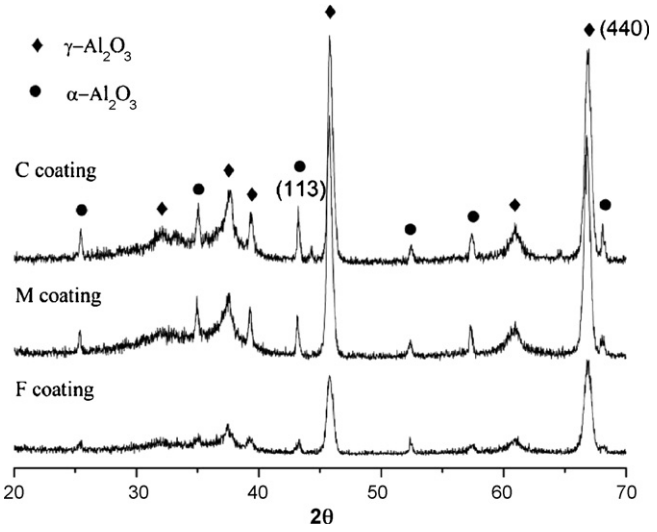

Fig. 5. XRD patterns of the as-sprayed coatings.

and, secondly, due to the reduced melting efficiency of coarser particles in plasma plume compared with fine particles. Generally, for the same materials, the larger particles tend to penetrate the core and travel around the periphery of the plasma jet for their larger inertia effects, while the position of smaller particles is near to the hot core of the plasma jet.[21] Therefore, the smaller particles can be easily accelerated and heated by the surrounding gas in the hot core of plasma jet. On the other hand, the larger the particle size, the higher total heat capacity, such that the larger particles need more time to be melted.[15] According to the results achieved by McPherson[22] the increase of particle size for the same materials will result in the increasing "difficulty of melting factor" DMF, due to the decreased residence time of particles in the high temperature zone of jet. Consequently, it is reasonable that the F particle, followed by M and C particles, possesses the highest in-flight temperature and velocity (Fig. 4).

3.2. X-ray diffraction analysis

The XRD patterns of the as-sprayed coatings showed that most of α-Al_2O_3 in the feedstock powders was converted into γ-Al_2O_3 after plasma spraying process, as presented in Fig. 5. It is well established that the preferential formation of γ-Al_2O_3 is attributed to the high cooling rate (about 10^6 K/s) of the molten particles during plasma spraying and easy nucleation of γ-Al_2O_3 from the melt superior to α-Al_2O_3 thanks to lower interfacial energy between crystal and liquid.[5] On the other hand, the phase composition of Al_2O_3 coating is shown to relate with the particle melting state.[7,12] It is suggested that the amount of the γ-Al_2O_3 in the plasma-sprayed Al_2O_3 coating can represent the particle melting extent. From the XRD analysis of the as-sprayed Al_2O_3 coatings, as shown in Fig. 5, it indicates that better particle melting extent can be achieved for the F coating in terms of its higher γ-Al_2O_3 amount suggested by lower ratio (17.5%) of the heights of {1 1 3}α and {4 4 0}γ peaks.[23]

3.3. Microstructural analysis

Typically, plasma-sprayed coatings contained porosity.[24] Characterization of polished cross-sections was useful to visualize internal microstructure of as-sprayed coatings, effectively providing the following information: the particle melting degree, an approximation of the porosity and pores morphology and distribution.[25] As shown in Fig. 6, the F coating stands out among the various coatings studied in this experiment to possess dense microstructure with low porosity, indicative of good particle melting.[7] Furthermore, it can be found that there are distinct differences in the pore or crack size, morphology and distribution within various coatings. Fig. 6(a) reveals that homogeneously distributed small spherical shape pore, most of which less than 3 μm, was found predominantly in F coating, whereas in M and C coatings, few aforementioned shape of pores can be observed, but some irregular large volumetric pores and cracks were identified. Especially for the C coating, the large volumetric pores are around or larger than 10 μm. The differences in microstructure manifest themselves as variations in the porosity levels in the coatings. The porosities of the as-sprayed coatings measured using SEM image analysis of the cross-section were 4.6%, 5.9% and 8.3%, respectively, as presented in Fig. 7. This suggests that such kind of large volumetric pore may be the main contribution to the total porosity of the coating and the increase in particle in-flight velocity and temperature (Fig. 4) can result in a smaller number of large volumetric pores and lower porosity within ultimate coating, which is in accordance with the findings of Friis et al.[19] and Kesler et al.[26]

3.4. Mechanical properties

Plasma-sprayed ceramic coatings have been widely used in industry for wear and erosion resistance.[27,28] In such

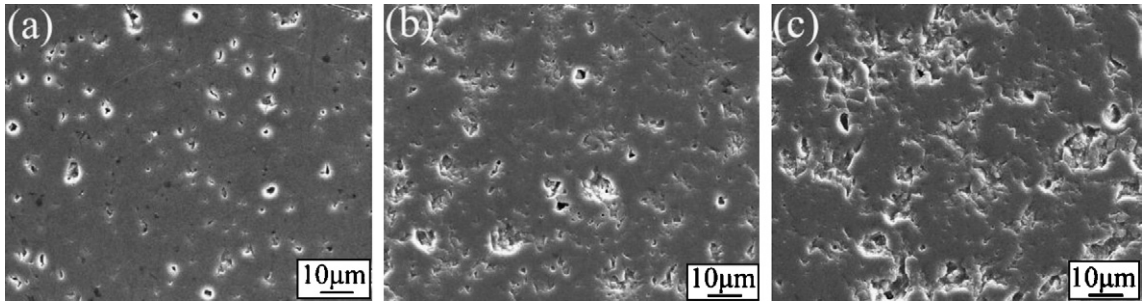

Fig. 6. Cross-sectional morphologies of the as-sprayed F (a), M (b) and C (c) coatings.

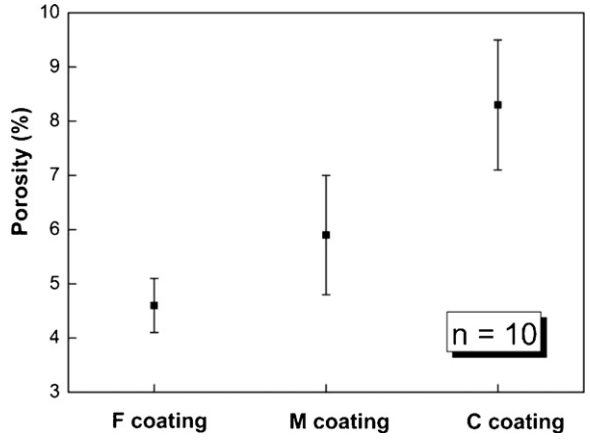

Fig. 7. Comparison of porosity for various coatings studied in this work. Standard deviation bars are added.

applications, the coatings need to experience intense mechanical loads and, hence, it is very necessary and useful to know their mechanical response for the prediction of appropriate operating conditions and service time. Fig. 8 illustrates the comparison of microhardness and adhesion strength for various coatings studied in this work. It shows that higher microhardness and adhesion strength can be obtained for the coating manufactured using the finer feedstock. As indicated in Fig. 8, F coating, among the three coatings used in this study, possesses the highest microhardness (982.5 $HV_{0.2}$) and adhesion strength (30.2 MPa). On the other hand, it can be seen that lower mechanical data scatter is attained for the F coating, which is closely linked to the homogeneity of coating microstructure. An additional statistic study of Weibull analysis[29,30] was employed to further examine the microstructural characteristics of coatings in light of microhardness variation. The Weibull plots of microhardness, as seen in Fig. 9, are approximate patterns of linearity and the smallest correlation coefficient (R) between the measured points and regressed line was 0.968. The value was much larger than the critical correlation coefficient 0.561 for a statistical test to assess whether a data set with a sample size of 20 significantly follows a regressed line under a confidence level of 0.99.[31] Compared with M and C coatings, the F coating exhibits larger Weibull modulus

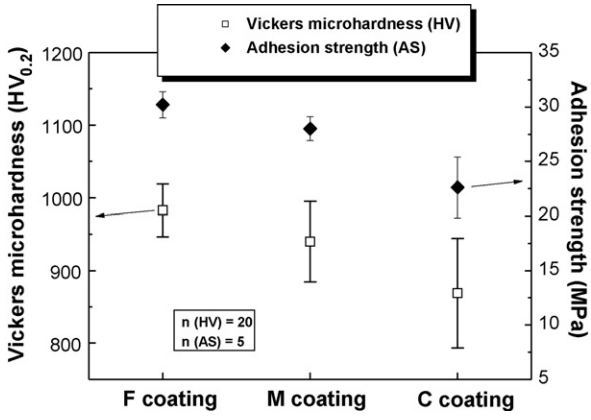

Fig. 8. Comparison of microhardness and adhesion strength of various coatings used in this study. Standard deviation bars are added.

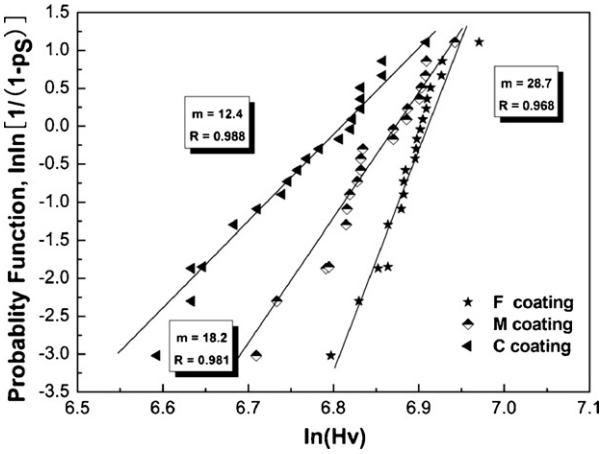

Fig. 9. Weibull plot of the microhardness for various coatings used in this study, where P_S is the probability of survival; m is the weibull modulus and R is correlation coefficient.

($m = 28.7$), indicative of its more homogeneous microstructure, as visualized in Fig. 6a.[29]

Numerous studies suggested that the mechanical property of plasma-sprayed coatings is closely related to its microstructure.[10,32] Plasma-sprayed coating develops by the successive impingement and inter-bonding among the splats (solidified individual particle). Deforming and spreading of the melting particles on the impact onto a substrate or previously deposited layer are mainly driven by the kinetic and thermal energy of in-flight particle, in connection with particle in-flight velocity and temperature.[10,33] As for the F particles, the improved kinetic and thermal energy of in-flight particles arising from their higher velocity and temperature effectively contribute to deposit densely stacked and well bonded splats resulting in compact microstructure and developed mechanical properties (Fig. 8). In contrast, because of relatively low velocity and temperature of larger feedstock like C particles, within resulting coating weakly bonded splats and inhomogeneous microstructure were observed (Fig. 6c). On the other hand, the increase in porosity is generally considered to decrease the mechanical properties of materials, as described in the following formula:[34]

$$S = S_0 \exp(-bP)$$

where S is the mechanical properties of sample, S_0 the mechanical properties of pore-free material, b the constant coefficient and P is the porosity of sample. Thus, the higher microhardness and adhesion strength of F coating can be attributed to its developed inter-bonding between splats and lower porosity.

4. Conclusions

In this work, the characteristics of three different grain fractions of Al_2O_3 feedstock was examined and compared in terms of their in-flight characteristics using the SprayWatch on-line monitoring system, with the aim of achieving better knowledge of the particle in-flight behavior—ultimate coating microstructure–mechanical properties relationship. It was found

that the particle in-flight behavior is strongly influenced by the feedstock powder size. The higher in-flight velocity and temperature can be obtained for the finer F particles compared with respect to M and C particles. Because of the improved in-flight behaviors and melting extent of small particles, these produce increasingly bonded splats resulting in coating with compact microstructure, where homogeneously distributed small spherical shape pores and low porosity were realized. The increased inter-bonding between splats and low porosity within F coating could well account for its higher mechanical properties. In contrast, larger particles exhibit lower in-flight velocity and temperature, resulting in weakly stacked and bonded coating with a certain amount of irregular large volumetric pores and relatively high porosity, in addition to lower microhardness and adhesion strength.

Acknowledgements

The authors wish to express their thanks to Ms. Zhenglan Lu and Weijun Qian for mechanical test and SEM analysis, and Dr. Xuanyong Liu and Youtao Xie for their constructive proposals and effective discussions during performing the present study.

References

1. Ctibor, P., Bohac, P., Stranyanek, M. and Ctvrtlik, R., Structure and mechanical properties of plasma sprayed coatings of titania and alumina. *J. Eur. Ceram. Soc.*, 2006, **26**, 3509–3514.
2. Kezelis, R. and Brinkiene, K., Effect of alumina addition on the microstructure of plasma sprayed YSZ. *J. Eur. Ceram. Soc.*, 2005, **25**, 2181–2184.
3. Sarikaya, O., Effect of some parameters on microstructure and hardness of alumina coatings prepared by the air plasma spraying process. *Surf. Coat. Technol.*, 2005, **190**, 388–393.
4. Chen, H., Ding, C. X., Zhang, P. Y., La, P. Q. and Lee, S. W., Wear of plasma-sprayed nanostructured zirconia coatings against stainless under distilled-water conditions. *Surf. Coat. Technol.*, 2003, **173**, 144–149.
5. McPherson, R., On the formation of thermally sprayed alumina coatings. *Mater. Sci.*, 1980, **15**, 3141–3149.
6. Dykhuizen, R. C., Review of impact and solidification of molten thermal spray droplets. *J. Therm. Spray Technol.*, 1994, **3**, 351–361.
7. Zhao, L. D., Seemann, K., Fischer, A. and Lugscheider, E., Study on atmospheric plasma spraying of Al_2O_3 using on-line particle monitoring. *Surf. Coat. Technol.*, 2003, **168**, 186–190.
8. Herold, T. G., Prask, H. J., Barker, J. *et al.*, Microstructure, mechanical properties and adhesion in IN625 air plasma sprayed coatings. *Mater. Sci. Eng. A*, 2006, **421**, 77–85.
9. Fang, J. C., Xu, W. J., Zhao, Z. Y. and Zeng, H. P., In-flight behaviors of ZrO_2 particle in plasma spraying. *Surf. Coat. Technol.*, 2007, **201**, 5671–5675.
10. Guessasma, S., Montavon, G. and Coddet, C., Velocity and temperature distributions of alumina–titania in-flight particles in the atmospheric plasma spray process. *Surf. Coat. Technol.*, 2005, **192**, 70–76.
11. Fukanuma, H., Ohno, N., Sun, B. and Huang, R., In-flight particle velocity measurements with DPV-2000 in cold spray. *Surf. Coat. Technol.*, 2006, **201**, 1935–1941.
12. Gao, Y., Xu, X. L., Yan, Z. J. and Xin, G., High hardness alumina coatings prepared by low power plasma spraying. *Surf. Coat. Technol.*, 2002, **154**, 189–193.
13. Lin, X. H., Zeng, Y., Lee, S. W. and Ding, C. X., Characterization of alumina–3wt% titania coating prepared by plasma spraying of nanostructured powders. *J. Eur. Ceram. Soc.*, 2004, **24**, 627–634.
14. Liang, B. and Ding, C. X., Thermal shock resistances of nanostructured and conventional zirconia coatings deposited by atmospheric plasma spraying. *Surf. Coat. Technol.*, 2005, **197**, 185–192.
15. Deshpande, S., Kulkarni, A., Sampath, S. and Herman, H., Application of image analysis for characterization of porosity in thermal spary coatings and correlation with small angle neutron scattering. *Surf. Coat. Technol.*, 2004, **187**, 6–16.
16. Boudi, A. A., Hashmi, M. S. J. and Yilbas, B. S., HVOF coating of inconel 625 onto stainless and carbon steel surfaces: corrosion and bonding testing. *J. Mater. Process. Technol.*, 2004, **155–156**, 2051–2055.
17. ASTM Designation C 633-79, Standard test method for adhesion or cohesive strength of flame sprayed coatings, 1979.
18. Westhoff, R., Trapaga, G. and Szekely, J., Plasma-particle interactions in plasma spraying systems. *Metall. Trans. B*, 1992, **23B**, 683–689.
19. Friis, M., Persson, C. and Wigren, J., Influence of particle in-flight characteristics on the microstructure of atmospheric plasma sprayed yttria stabilized ZrO_2. *Surf. Coat. Technol.*, 2001, **141**, 115–127.
20. Wan, Y. P., Sampath, S., Prasad, V., Williamson, R. and Fincke, J. R., An advanced model for plasma spraying of functionally graded materials. *J. Mater. Process. Technol.*, 2003, **137**, 110–116.
21. Smith, W., Jewett, T. J., Sampath, S., Swank, W. D. and Fincke, J. R., In *Thermal Spray: A United Forum for Scientific and Technological Advances*, ed. C. C. Berndt. ASM International, Materials Park, OH, 1997, pp. 599–605.
22. McPherson, R., The relationship between the mechanism of formation, microstructure and properties of plasma-sprayed coatings. *Thin Solid Films*, 1981, **83**, 297–310.
23. Guilemany, J. M., Nutting, J. and Dougan, M. J., A transmission electron microscopy study of the microstructures present on alumina coatings produced by plasma spraying. *J. Therm. Spray Technol.*, 1997, **6**, 425–429.
24. Kulkarni, A., Gutleber, J. *et al.*, Studies of the microstructure and properties of dense ceramic coatings produced by high-velocity oxygen-fuel combustion spraying. *Mater. Sci. Eng. A*, 2004, **369**, 124–137.
25. Harmsworth, P. D. and Stevens, R., Phase composition and properties of plasma-sprayed Zirconia thermal barrier coatings. *J. Mater. Sci.*, 1992, **27**, 616–624.
26. Kesler, O., Matejicek, J., Sampath, S., Suresh, S., Gnaeupel-Herold, T., Brand, P. C. and Prask, H. J., Measurement of residual stress in plasma-sprayed metallic, ceramic and composite coatings. *Mater. Sci. Eng. A*, 1998, **257**, 215–224.
27. Xie, Y. and Hawthorne, H. M., Wear mechanism of plasma-sprayed alumina coating in sliding contacts with harder asperities. *Wear*, 1999, **225–229**, 90–103.
28. Fervel, V., Normand, B. and Coddert, C., Tribological behavior of plasma sprayed Al_2O_3-based cermet coatings. *Wear*, 1999, **230**, 70–77.
29. Lima, R. S., Kucuk, A. and Berndt, C. C., Bimodal distribution of mechanical properties on plasma sprayed nanostructured partially stabilized zirconia. *Mater. Sci. Eng. A*, 2002, **327**, 224–232.
30. Li, J. F. and Ding, C. X., Determining microhardness and elastic modulus of plasma-sprayed Cr_3C_2–NiCr coatings using Knoop indentation testing. *Surf. Coat. Technol.*, 2001, **135**, 29–237.
31. Sturgeon, A. J. *et al.*, In *ITSC-95 Conference Proceedings, vol. 2*, 1995, pp. 669–673.
32. Safai, S. and Herman, H., Microstructural investigation of plasma sprayed aluminum coatings. *Thin Solid Films*, 1977, **45**, 295–307.
33. Li, C. J. and Sun, B., Effect of spray parameters on the microstructure and property of Al_2O_3 coatings sprayed by a low power plasma torch with a novel hollow cathode. *Thin Solid Films*, 2004, **450**, 282–289.
34. Li, C. J. and Ohmori, A., Relationships between the microstructure and properties of thermally sprayed deposits. *J. Therm. Spray. Technol.*, 2003, **11**, 365–374.